Biosensors and Bioelectronics 179 (2021) 113077

Contents lists available at ScienceDirect

Biosensors and Bioelectronics

journal homepage: http://www.elsevier.com/locate/bios

Plasma membrane anchored nanosensor for quantifying endogenous production of H_2O_2 in living cells

Shigekuni Hosogi [a,b], Yoshinori Marunaka [b,c,d], Eishi Ashihara [a], Tadaaki Yamada [e], Ayumi Sumino [f,g], Hideo Tanaka [h], Leonardo Puppulin [f,h,*]

[a] Department of Clinical and Translational Physiology, Kyoto Pharmaceutical University, Misasagi, Yamashina-ku, Kyoto, 607-8414, Japan
[b] Department of Molecular Cell Physiology, Graduate School of Medical Sciences, Kyoto Prefectural University of Medicine, Kajii-cho, Kawaramachi-Hirokoji, Kyoto, 602-8566, Japan
[c] Research Center for Drug Discovery and Pharmaceutical Development Science, Research Organization of Science and Technology, Ritsumeikan University, Kusatsu, 525-8577, Japan
[d] Research Institute for Clinical Physiology, Kyoto Industrial Health Association, 67 Kitatsuboi-cho, Nishino-kyo, Nakagyo-ku, Kyoto, 604-8472, Japan
[e] Department of Pulmonary Medicine, Graduate School of Medical Sciences, Kyoto Prefectural University of Medicine, Kajii-cho, Kawaramachi-Hirokoji, Kyoto, 602-8566, Japan
[f] WPI Nano Life Science Institute (WPI-NanoLSI), Kanazawa University, Kakumamachi, Kanazawa, 920-1192, Japan
[g] Institute for Frontier Science Initiative, Kanazawa University, Kakumamachi, Kanazawa, 920-1192, Japan
[h] Department of Pathology and Cell Regulation, Graduate School of Medical Sciences, Kyoto Prefectural University of Medicine, Kajii-cho, Kawaramachi-Hirokoji, Kyoto, 602-8566, Japan

ARTICLE INFO

Keywords:
Hydrogen peroxide
Nanosensor
Redox biology
Gold nanoparticles
Surface enhanced Raman spectroscopy
NADPH-Oxidase
4-Mercaptophenylboronic pinacol ester

ABSTRACT

Hydrogen peroxide (H_2O_2) is one of the main second messengers involved in signaling pathways controlling cell metabolism. During tumorigenesis H_2O_2 is generated on the extracellular space by membrane-associated NADPH oxidases and superoxide dismutase to stimulate cell proliferation and preservation of the transformed state. Accordingly, a characteristic feature of malignant cells is overproduction of H_2O_2 in the extracellular milieu and the subsequent absorption in the cytosol. Since the most significant gradients of endogenous extracellular H_2O_2 can be observed only in a very shallow region of the fluid in contact with the plasma membrane, we show here the use of a newly designed nanosensor anchored to the outer cell surface and capable of quantifying H_2O_2 at nanometer distance from the membrane proteins responsible for its production. This biosensor is built upon gold nanoparticles functionalized with a H_2O_2-sensitive boronate compound that is probed using surface enhanced Raman spectroscopy (SERS). The highly localized information obtained on the cell surface by SERS analysis is combined with analytical methods of redox biology to estimate the associated levels of intracellular H_2O_2 responsible for cell signaling. The results obtained from A549 lung cancer cell line show localized spots on the cell surface at concentration up to 12 μM, associated to intracellular concentration up to 5.1 nM.

1. Introduction

Several physiological and pathological responses that are observed and studied in mammalian cells are triggered and regulated by redox reactions. Within this specific category of biological reactions, one pivotal role is played by the reduction of oxygen that leads to the formation of radical and non-radical oxygen species, also known as reactive oxygen species (ROS). As a matter of fact, ROS are involved in diverse biological processes, including cell proliferation, apoptosis, antibacterial defense and oxygen sensing (Behrend et al., 2003; Burdo and Rice-Evans 1989; Cash et al., 2007; D'Autréaux and Toledano 2007; Finkel 2011; Simon et al., 2000; Stone and Yang 2006). It has been demonstrated that they regulate mitogen-activated protein kinases (MAPKs) that are essential in signal transduction from the cell membrane to the nucleus (Son et al., 2011). As far as the study of abnormal physiological conditions is concerned, the alteration of ROS metabolism has been identified in different pathologies, such as inflammation, vascular atherosclerosis, diabetes, hypertension, and tumorigenesis (Gupta et al., 2012; Paravicini and Touyz 2008; Taniyama and Griendling 2003; Touyz 2005). Cancer cells are thought to function in the

* Corresponding author. WPI Nano Life Science Institute (WPI-NanoLSI), Kanazawa University, Kakumamachi, Kanazawa, 920-1192, Japan.
E-mail address: puppulin@staff-kanazawa-u.ac.jp (L. Puppulin).

https://doi.org/10.1016/j.bios.2021.113077
Received 14 October 2020; Received in revised form 12 January 2021; Accepted 4 February 2021
Available online 10 February 2021

presence of higher levels of oxidative species than normal cells (Liou and Storz 2010; Waris and Ahsan 2006). Malignant cells use ROS for maintenance of the transformed state and for autocrine proliferation signaling (Behrend et al., 2003; Fruehauf and Meyskens 2007). One of the most abundant type of ROS in cells is hydrogen peroxide (H_2O_2), which has a central importance in various physiological and pathophysiological processes due to its peculiar combination of stability and oxidizing strength (Brandes et al., 2014; Groeger et al., 2009; Panday et al., 2015; Ushio-Fukai and Nakamura 2008). In fact, as compared to the other ROS, at moderate concentration, its longer lifetime makes H_2O_2 a potent and widely exploited secondary messenger, while, at higher concentration, it becomes a lethal oxidant. The dual antithetical role of H_2O_2 is therefore dependent on its concentration, which must be tightly regulated by cells to guarantee their survival and correct functioning. For example, in cancer cells the extracellular tendency to produce H_2O_2 is limited by over-expression of antioxidants, such as membrane associated catalase, which prevent the initiation of ROS-mediated signaling leading to apoptosis (Bauer 2012; Scheit and Bauer 2015). Conversely, new therapeutic approaches can be engineered by targeting malignant cells to raise their level of H_2O_2 over the threshold that causes irreversible damage (Chen et al., 2011; Gorrini et al., 2013; Schumacker 2015; Trachootham et al., 2006). In light of these considerations, the quantification of actual H_2O_2 concentrations that activate specific signaling pathways or induce cell death is fundamental to fully elucidate physiological processes or to tailor new therapeutic strategies. In the past two decades, the amelioration of the experimental tools to collect quantitative information in biological samples fostered the growth of redox biology as an analytical science (Lyublinskaya et al., 2017). The seminal study of Antunes and Cadenas (2000) provided the basics to estimate H_2O_2 gradients between extracellular and intracellular compartments. It mainly relies on the calculation of the kinetic parameters describing H_2O_2 absorption across the plasma membrane and the redox reactions with the antioxidants of the intracellular space. These tasks can be accomplished by monitoring the variation of emission of fluorescence probes upon addition of exogenous H_2O_2 to specifically prepared cell samples (Antunes and Cadenas 2000; Huang and Sikes 2014). Nonetheless, although gradients can be estimated, the actual basal levels of H_2O_2 cannot be precisely quantified unless highly localized measurements of extracellular or intracellular H_2O_2 are collected in physiologically relevant conditions. Nowadays, the most advanced and accurate assay to directly quantify H_2O_2 in the cytosol is based on genetically encoded redox biosensors (Belousov et al., 2006; Huang et al., 2016; Huang and Sikes 2014; Lyublinskaya and Antunes 2019; Sies 2017), which are still cumbersome to handle and they require long sample preparation and careful calibration. In this study, we report the use of bioconjugated gold nanoparticles (AuNP) combined with surface enhanced Raman spectroscopy (SERS) to estimate concentrations of endogenous extracellular hydrogen peroxide ($[H_2O_2]_e$) localized on the cell surface with nanometer scale resolution. We exploit and adapt an experimental approach that we previously validated to anchor gold nanoaggregates to the outer membrane of cells (Puppulin et al., 2018). For the purpose of the present study, the nanosensor is coated with H_2O_2-sensitive 4-mercaptophenylboronic acid pinacol ester (4MPBE). The intensities of specific Raman bands associated to the boronate compound show selective dependence upon exposure to different concentrations of H_2O_2, which enables us to calibrate the nanosensor anchored to the cells. The proposed method is tested on adenocarcinomic human alveolar basal epithelial cells (i.e., A549 cell line). In addition, we show here that the quantification of $[H_2O_2]_e$ by SERS enables us to estimate also the correlated concentration of intracellular hydrogen peroxide ($[H_2O_2]_i$) using the typical transmembrane gradient obtained with advanced methods of redox biology.

2. Experimental section

2.1. A549 cell culture

Human lung adenocarcinoma A549 cells were obtained from ATCC. We seeded the cells into 25 cm^2 flasks at a density of 2.5×10^5 cells/flask and incubated for 24 h in RPMI 1640 medium (Sigma-Aldrich, MO, USA) supplemented with 5% fetal bovine serum (FBS) in a humidified incubator at 37 °C with 5% CO_2 in air. The culture medium was changed every 3 days.

2.2. Preparation of bioconjugated AuNP

We adapted the experimental protocol reported in our previous work (Puppulin et al., 2018) by substituting the pH-sensitive compound (i.e., 4-mercaptobenzoic acid) with the H_2O_2-sensitive 4MPBE. We used as gold nano-substrate the commercially available 90 nm gold nano-urchins in 0.1 mM PBS (Sigma Aldrich, St. Louis, Missouri, USA). We dissolved N-(6-(Biotinamido)hexyl)-3′-(2′-pyridyldithio)-propionamide (EZ-link -HPDP-Biotin, Thermo Scientific, MA, USA) in DMSO to prepare a 10 μM stock solution. The compound 4MPBE (1 mM stock solution) was obtained upon overnight incubation of 4-mercaptophenylboronic acid (Sigma Aldrich, MO, USA) with pinacol (1:2 ratio in ethanol). Self-assembled monolayers of 4MPBE and EZ-link-HPDP-Biotin on AuNP were prepared by adding 50 μL 4MPBE stock solution +10 μL HPDP-B stock solution to 1 mL of AuNP colloidal solution, which were incubated for 30 min at 21 °C using a rotating mixer. Separation of AuNP was obtained by 30 min centrifugation at 250*g*, which was repeated on the supernatant for 30 min at 1000 g. The AuNP were resuspended in 1 mL RPMI 1640 medium (without phenol red, Wako Pure Chemical Corporation, Osaka, Japan) before incubation on cells seeded on a glass bottom dish and pre-treated as explained in the following paragraph.

2.3. Cell surface labelling with bioconjugated AuNP

Cells seeded on a glass bottom dish were placed at 4 °C for 10 min and rinsed twice with ice-cold 0.01 M PBS +2 mM $CaCl_2$/1 mM $MgCl_2$ at pH 7.4 (hereafter referred as PBS-2Ca). We labelled the cell surface proteins with the biotinylation reagent EZ-link Sulfo–NHS–SS-Biotin (100 mg powder, Thermo Scientific, MA, USA). We treated each dish with 1 mg NHS–B in 1 mL PBS-2Ca at pH 8.0 for 30 min at 4 °C. After rinsing with ice-cold PBS-2Ca (3 times per 3 min), we added 200 μL of 10 μM streptavidin (Sigma Aldrich, MO, USA) in 1 mL PBS-2Ca at pH 7.4 for 30 min at 4 °C. Following rinsing in PBS-2Ca, the cells were incubated with 1 mL of bioconjugated AuNP colloidal solution for 15 min at 4 °C followed by 15 min at 21 °C. Robust washing with 0.01 M PBS for 5 times was the final step before SERS analysis. During the spectroscopic analyses we used RPMI 1640 medium solution without phenol red.

2.4. Cytotoxicity assay

A549 cells were seeded onto a 96-well plate and incubated for 48 h. Six wells were treated for AuNP anchoring to the outer membrane surface and 6 wells were used as control. Cell viability was measured by MTT assay. Briefly, 6 mg of MTT were dissolved in 1.2 mL isotonic buffer solution and in each well 200 μL were added for 3 h. Then buffer solution was replaced with DMSO to dissolve blue formazan crystals, and plate was shaken for 15 min in the dark. Results were obtained by measuring the absorbance at 570 nm using an automated micro plate reader (SpectraMax M2e, Molecular Devices, San Jose, CA, USA). Assuming the mean viability of the control samples as 100%, the mean cell viability of samples treated with the nanosensor was expressed as percentage of control.

2.5. AFM imaging

AFM analysis was performed using Cypher (Asylum Research) with AC mode. The cantilever used was the BL-AC40TS with a tip radius of ~7 nm, the resonant frequency in buffer solution of 25 kHz, and the spring constant of 0.09 N/m. The AFM imaging was performed on A549 cells in buffer solution after AuNP anchoring and fixation with 2.5% glutaraldehyde/2% paraformaldehyde (GA-PA) in 0.1 M PBS for 30 min at 21 °C.

2.6. SERS analysis

Spectra were collected using a Raman microscope (Raman-11, Nanophoton, Osaka, Japan), equipped with a 671 nm laser excitation source (Ignis, Laser Quantum, Manchester, UK), a 60 × water immersion objective lens of NA = 1.1 (Olympus, Tokyo, Japan) and a 600 grooves/mm diffraction grating. The in-plane spot size of the laser probe was estimated in 700 nm (Puppulin et al., 2018). For in vitro analysis of A549 cells, we analyzed cell samples after 1-h incubation in RPMI 1640 medium with and without addition of Diphenyleneiodonium chloride (DPI, 10 μM). For each of the two cases, we collected in-plane xy raster scans of points with 1 μm steps on the surface of three cells of three different cultures. The laser power and acquisition time for each spectrum were set to 2.4 mW and 5 s, respectively. We also performed experiments on n = 3 A549 cells treated with the pH-sensitive nanosensor reported in our previous work (Puppulin et al., 2018). The acquisition of each map started 60 min after the completion of the cell labelling with AuNP. For the calibration of the nanosensor, we collected Raman spectra from AuNP anchored to the outer surface of cells, after incubation at constant concentration of H_2O_2 for 1 h. In detail, H_2O_2 solution of 30% (w/w) in H_2O (Wako Pure Chemical Corporation, Osaka, Japan) was diluted at different concentrations. After the completion of the protocol for AuNP labelling, the cells were fixed with GA-PA in 0.1 M PBS, rinsed three times with RPMI 1640 buffer solution and incubated at room temperature for 1 h at a constant concentration of H_2O_2 in buffer solution (pH 6.7). During the incubation time, we changed the H_2O_2 solution four times to ensure that AuNP were constantly exposed to the same concentration of H_2O_2. For each concentration, we analyzed two samples and collected a total number of ten spectra. The laser power and acquisition time for each spectrum were set to 2.4 mW and 5 s, respectively. The results reported in Figure A1 of Appendix A confirmed the stability of 4MPBE SAM exposed to the selected laser power output. Spectral Raman lines were analyzed and deconvoluted using a commercially available software package (Origin 9.1, OriginLab Co., MA, USA). Fitting of intensity bands was performed using Gaussian-Lorentzian (i.e., Voigtian) functions after baseline subtraction.

2.7. Solutions containing biologically relevant species

Buffer solutions (pH 7.4) containing superoxide ($O_2^{\cdot-}$, 100 μM) were prepared dissolving KO_2 (Sigma Aldrich MO, USA). Buffer solutions containing tert-butyl hydroperoxide (TBHP, 100 μM) were prepared using 5 M stock solution of TBHP in decane (Sigma Aldrich MO, USA). Buffer solutions containing 100 μM hypochlorite ion (OCl^-) were prepared using 5% sodium hypochlorite solution (Sigma Aldrich MO, USA). Buffer solutions containing 100 μM nitric oxide (·NO) were prepared from stock solution of S-Nitroso-N-acetyl-DL-penicillamine (SNAP, Sigma Aldrich MO, USA) dissolved in DMSO. Hydroxyl radicals (OH·) were generated by reaction of 1 mM of Fe^{2+} (Ammonium iron(II) sulfate hexahydrate, Sigma Aldrich MO, USA) with 100 μM H_2O_2. The effect of different concentrations of peroxynitrite (PN) on the nanosensor was studied using a stock solution of 2 mM PN in sodium hydroxide (NaOH, Nakalai Tesque, Kyoto, Japan) prepared with sodium nitrite ($NaNO_2$, Nakalai Tesque, Kyoto, Japan), H_2O_2, HCl (Wako Pure Chemical Corporation, Osaka, Japan) and NaOH, according to the method reported in (Robinson and Beckman 2005). The concentration of the stock was quantified measuring the absorption at 302 nm and using the extinction coefficient equal to 1700 M^{-1} cm^{-1}. The influence of glucose (Glu, D (+)-Glucose, Nakalai Tesque, Kyoto, Japan), glutathione (GSH, L-glutathione reduced, Sigma Aldrich MO, USA), albumin (Alb, Wako Pure Chemical Corporation, Osaka, Japan) and fructose (Fru, D (−)-Fructose, Wako Pure Chemical Corporation, Osaka, Japan) was verified in buffer solutions at concentrations of 5 mM, 2 mM, 5% and 5 mM, respectively.

2.8. Kinetic of H_2O_2 adsorption across plasma membrane in A549 cells

The kinetic of extracellular H_2O_2 absorption by intact A549 cells was studied following protocols previously reported (Huang and Sikes 2014). We suspended A549 cells in 10 mL PBS buffer solution with 2 g L^{-1} d-glucose at a concentration of 10^6 cells mL^{-1}. We added 100 μL of 10 mM H_2O_2 to the cell suspension to expose the cell to a total H_2O_2 concentration of 100 μM. We retrieved the standard curve of H_2O_2 consumption between 0 and 100 μM by systematically collecting and analyzing 200 μL cell s-uspension every 2 min. Every collected sample was inactivated with 13 μL 5 N HCl and centrifuged at 14000 g. The supernatant (160 μL) was mixed with 70 μL of 1 M potassium phosphate buffer (pH = 8.0), 50 μL of 2.5 mM solution of 2,2′-azino-bis(3-ethylbenzothiazoline-6-sulfonic acid) (ABTS, Nacalai Tesque, Inc., Japan) and 10 μL of 3 mg mL^{-1} of horse-radish peroxidase (Tokyo Chemical Industry Co., Ltd. (TCI), Japan). The concentration of H_2O_2 was calculated from the absorbance read at the wavelength of 405 nm.

2.9. Kinetic of H_2O_2 consumption by 2-cys peroxiredoxins in A549 cells

The kinetic of reaction of H_2O_2 with intracellular 2-cysteine peroxiredoxins was studied following protocols reported in (Huang and Sikes 2014). A549 cells (6 million mL^{-1}) were lysed in 20 mM Hepes (pH 7.4), 1 mM EDTA buffer containing 0.1% Triton solution. The lysate mixture was pre-incubated at 37 °C with 15 μM human thioredoxin (Trx1, human recombinant, Cayman Chemical, USA), 2 μM thioredoxin reductase (TrxR rat recombinant, Cayman Chemical, USA), 300 μM NADPH (Nacalai Tesque, Inc., Japan) and 1 mM NaN_3 (Nacalai Tesque, Inc., Japan) for 30 min. NADPH depletion after addition of a bolus of H_2O_2 was monitored by measuring the absorbance at 340 nm (extinction coefficient 6.22 mM^{-1} cm^{-1}). We performed experiments at two different initial concentrations of H_2O_2 after addition of the bolus, which were 20 and 25 μM. The experimental data were fitted using the set of differential equations proposed in (Huang and Sikes 2014), using the software *Mathematica* (Wolfram Research, Inc). More details can be found in Appendix A. The outcome of the fitting is the pseudo-first order rate constant k_{prx} that was used to estimate the typical H_2O_2 gradient across A549 cell membrane.

2.10. Statistical analysis

Statistical analysis was performed using Origin 9.1 (OriginLab Co., MA, USA). For biosensor calibration, at least n = 10 replicates were performed at each concentration of H_2O_2. Linear fitting was performed to correlate H_2O_2 concentration as a function of ratio of selected Raman band intensities. The influence of different reactive species on the nanosensor was validated comparing mean ratios of selected Raman band intensities using one-way ANOVA with Tukey's post hoc test ($n \geq 6$, significance level $\alpha = 0.05$). Results of MTT assay to verify cell viability were compared by two-sample t-test. The kinetic of peroxiredoxin was estimated by the results of n = 3 experiments on cell lysates with initial $[H_2O_2] = 20$ μM and n = 3 experiments on cell lysates with initial $[H_2O_2] = 25$ μM. The absorption of H_2O_2 across the membrane of intact cells was estimated from n = 6 experiments. Data are reported as the mean ± standard deviation (SD).

3. Results and discussion

3.1. Nanosensor design

The implementation of this nanosensor for H_2O_2 estimation in cells is based on the experimental methodology that we recently conceived and validated for the measurement of cell surface pH (Puppulin et al., 2018). The first stages of the design process consist of the choice and optimization of the molecular compounds to assemble on the nanostructure, followed by the study of the SERS spectrum and the confirmation of its sensitivity to H_2O_2. Fig. 1a shows an explanatory schematic of the nanosensor, whose capability of anchoring to the ectodomain of proteins on the cell surface was demonstrated by several experimental evidences reported in our previous work (Puppulin et al., 2018). The high resolution AFM images from A549 cells reported in Fig. 1b–d are further confirmation of the successful labelling of the surface with gold nanoaggregates. The conjugation of AuNP is specifically designed to fulfill two fundamental requirements: i) the efficient labelling of the outer membrane surface taking advantage of the strong affinity between biotin and streptavidin; ii) the quantification of H_2O_2 by detecting the Raman scattering of 4MPBE. We achieved the AuNP anchoring to the membrane using two molecular compounds containing biotin: a pyridyldithiol-biotin compound (HPDP-B), which conjugates to AuNP via thiol-gold interaction, and a sulfo–NHS–ester-biotin compound (NHS–B) that reacts with the primary amines of lysine and the amino-termini of protein ectodomains. The addition of streptavidin provides the strong and selective bond between biotinylated AuNP and membrane proteins. The results of MTT assay reported in Fig. 1e confirmed that cells cultures after treatment for nanosensor anchoring did not show statistically meaningful reduction of cell viability as compared to control samples (two-sample t-test, $p = 0.152$). At present, the majority of the molecular probes developed for selectively sensing

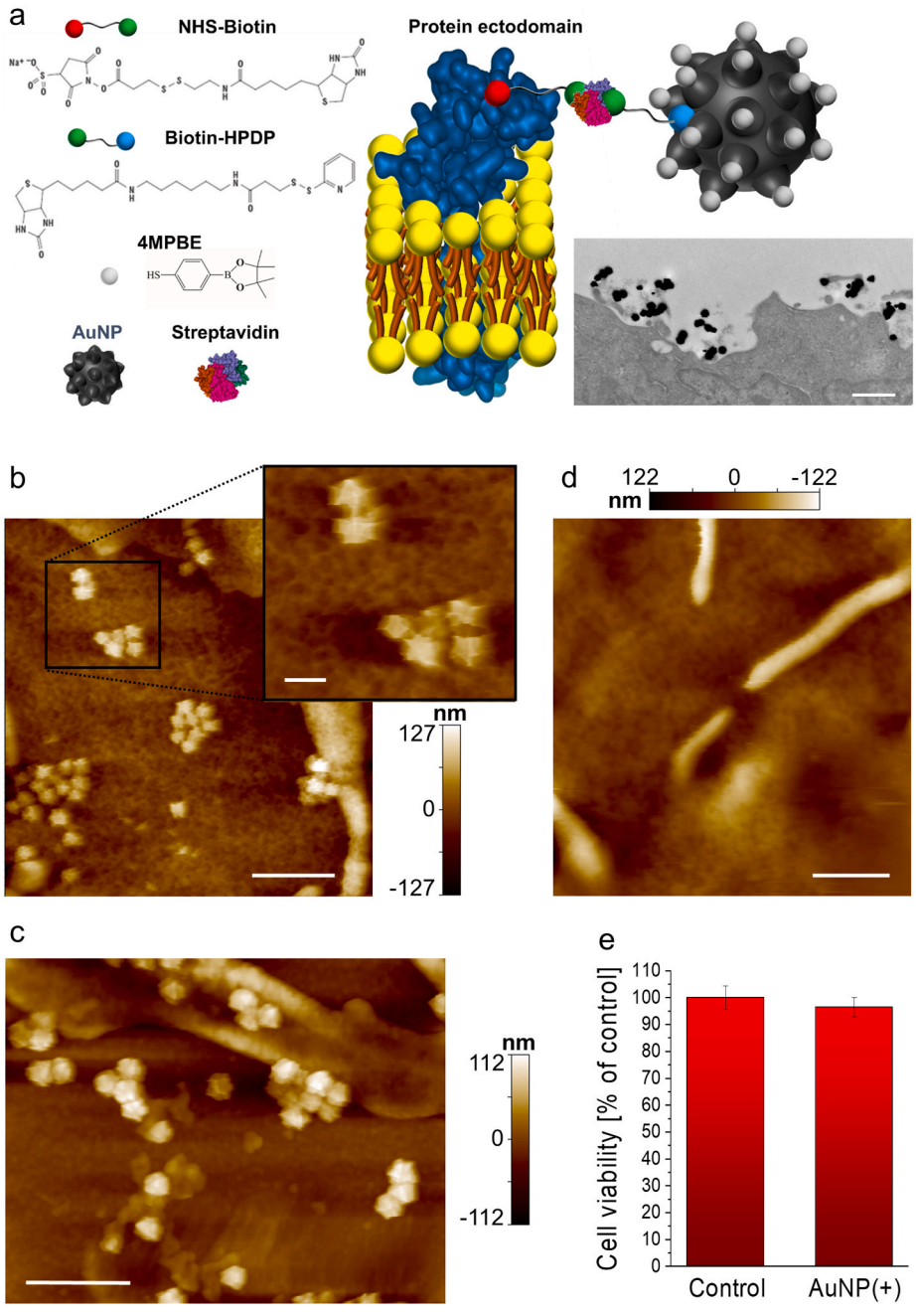

Fig. 1. Plasma membrane anchored nanosensor. a) Explanatory sketch of the plasma membrane anchored nanosensor. The compounds used for AuNP conjugation are 4MPBE and Biotin-HPDP. Biotinylation of the plasma membrane ectodomains is obtained using Sulfo–NHS–SS-Biotin. The anchoring of the conjugated AuNP to Sulfo–NHS–SS-Biotin is given by Streptavidin, reacting with the two biotin moieties. TEM imaging was performed in one of our previous studies (Puppulin et al., 2018) and it confirmed the effectiveness of this method for AuNP anchoring to the outer cell surface. b) and c) AFM images confirming the presence and the in-plane distribution of the nanosensor on the surface of A549 cells. The high-definition spiny morphology of the nano-urchins used as AuNP can be clearly observed in the magnified area of the inset in b). d) For comparison, typical AFM image of the cell surface with microvilli, collected from a control sample of untreated A549 cells. e) MTT assay results reported as percentage of living cells with respect to the average of the control samples (two-sample t-test, p = 0.152, error bars show SD). Scale bars: 500 nm, except for the inset in b), in which is 100 nm.

H_2O_2 in aqueous solutions are derived from aryl boronates, which are oxidized upon exposure to H_2O_2 (Cheng et al., 2020; Lin et al., 2013; Lippert et al., 2011; Miller et al., 2005; Peng et al., 2016; Qu et al., 2016). The molecular structure modification induced by this reaction can be correlated to the concentration of H_2O_2 in solution and quantified by the increase of absorptive/emissive properties of the compound (i.e., using fluorescence spectroscopy) or by the variation of inelastic scattering of selected photons of the compound (i.e., using Raman spectroscopy). As compared to the other ROS involved in cell biology, the selectivity of the reaction between H_2O_2 and aryl boronates is due to their peculiar nature of reactivity, which is ambiphilic. In fact, these two reagents have the specific ability to interact with each other in a complementary manner either as a two-electron electrophilic oxidant or a nucleophile, which enhances their affinity and it is not observed in other ROS (Jencks and Carriuolo 1960; Lippert et al., 2011). The aryl-boronate ester 4MPBE used to create our nano-sensor is synthesized from the reaction of 4-mercaptophenylboronic acid (4MPBA) and pinacol. This compound was selected for the ability to form a homogeneous self-assembled monolayer (SAM) on the surface of the nanostructures via gold-thiol interaction and for the strong Raman scattering, which is enhanced by surface plasmon polaritons generated upon illumination with a monochromatic laser source at 671 nm. Fig. 2a summarizes the reaction steps that modify the 4MPBE SAM on the gold surface after exposure to H_2O_2, leading to the formation of 4-mercaptophenols (4MPh). In Fig. 2b is reported the typical SERS spectrum obtained from colloidal solutions of our nanosensor after conjugation with 4MPBE and HPDP-B. The concentration of HPDP-B is 1000 times lower than the concentration of 4MPBE, purposely calibrated in order to guarantee the nanosensor anchoring to the cell surface without interference of the HPDP-B Raman scattering on the intensity of the collected SERS spectrum (Puppulin et al., 2018). The assignments of the SERS bands labelled in Fig. 2b are reported in Table 1 and they are merely associated to 4MPBE vibrational modes. The exposure of conjugated AuNP for 15 min to solutions with increasingly higher concentrations of H_2O_2 unequivocally induces progressive variation of the SERS spectrum, as shown in Fig. 2c. In 1 mM H_2O_2 solution, the SERS spectrum coincides with the spectrum collected from colloidal solution of AuNP conjugated with 4MPh. The assignments of the 4MPh bands labelled in Fig. 2c are reported in Table 1. This experimental evidence confirms the reaction scheme explained in Fig. 2a. All the spectra are normalized to the peak intensity of the band assigned to in-plane aromatic ring breathing mode 1 (Wilson notation) coupled with the CS stretching mode. This band is located at 1074 cm^{-1} in 4MPBE (Li et al., 2015; Sun et al. 2014, 2015) or 1076 cm^{-1} in 4MPh (Ji et al., 2011; Lee et al., 1994) (i.e., band labels 3 in Figs. 2b and 12 in Fig. 2c, respectively). The spectral features of 4MPBE that undergo to the most striking modification upon H_2O_2 exposure are the bands at 998 and 1022 cm^{-1} (i.e., band labels 1 and 2 in Fig. 2b), which we assigned to 12 and 18a ring vibrations, respectively. These assignments are in agreement with Sun et al. (2014, 2015), that reported the enhanced intensity of these two bands upon 4MPBA reaction with fructose, which is similar to the reaction of 4MPBA with pinacol to form 4MPBE. Differently, Peng et al. assigned the H_2O_2-sensitive band observed at 993 cm^{-1} to the B–O symmetric stretching (Peng et al., 2016). In the spectrum of 4MPh, we can notice the disappearance of the vibrational mode 12 and the onset of the mode 18a at 1004 cm^{-1}(i.e., band label 11 in Fig. 2c). The totally and non-totally symmetric ring-stretching modes 8a and 8b are observed in both 4MPBE (i.e., 1575 and 1584 cm^{-1}, band labels 9 and 10 in Fig. 2b) and 4 MPh (i.e., 1576 and 1592 cm^{-1}, band labels 16 and 17 in Fig. 2c). The redistribution of the intensity enhancement between these two vibrational modes is also correlated to charge-transfer enhancement mechanisms that occur in molecules with a π-system, such as benzene-like derivatives absorbed on metal surface (Centeno et al., 2012; Ji et al., 2011). Conversely, the previously mentioned mode 1 coupled with CS stretching at 1074 cm^{-1} is not affected by charge-transfer effect (Centeno et al., 2012), namely it can be reliably used as an internal standard to normalize the SERS spectra of both unmodified and H_2O_2-modified SAM. Similarly to 4MPBE, 4-mercaptoboronic acid (4MPBA) reacts with

Table 1
Assignments of the bands of the Raman spectra shown and labelled in Fig. 2b and c.

Frequency [cm^{-1}]	Assignment*	Reference	Figure label
4MPBE			
998	12	(Li et al., 2015; Sun et al. 2014, 2015)	*1*
1022	18a	[1,2]	*2*
1074	1	[1,2]	*3*
1112	15	Li et al. (2015)	*4*
1180	9a	Li et al. (2015)	*5*
1282	3	Li et al. (2015)	*6*
1472	19b	Sun et al. (2014)	*7*
1486	19a	(Li et al., 2015; Sun et al. 2014, 2015)	*8*
1575	8b	(Sun et al. 2014, 2015)	*9*
1584	8a	(Li et al., 2015; Sun et al. 2014, 2015)	*10*
4MPh			
1004	18a	(Ji et al., 2011; Lee et al., 1994)	*11*
1076	1	(Ji et al., 2011; Lee et al., 1994)	*12*
1167	9b	Ji et al. (2011)	*13*
1278	3	(Ji et al., 2011; Lee et al., 1994)	*14*
1485	19b	Ji et al. (2011)	*15*
1576	8b	(Ji et al., 2011; Lee et al., 1994)	*16*
1592	8a	(Ji et al., 2011; Lee et al., 1994)	*17*
*Wilson notation			

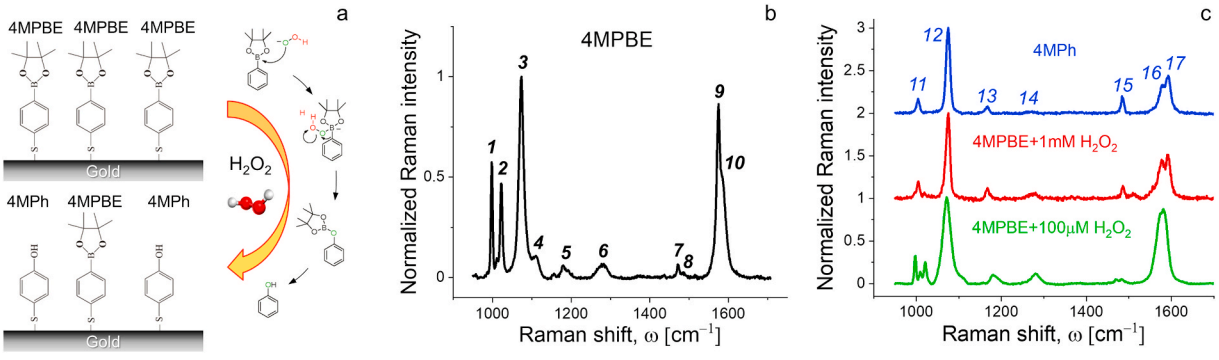

Fig. 2. 4MPBE SAM modification by H_2O_2 and SERS response. a) Reaction scheme explaining the modification of the 4MPBE SAM upon exposure to H_2O_2 (i.e., hydrogen peroxide anions, HO_2^-), leading to the formation of 4MPh. b) Typical SERS spectrum of the nanosensor after conjugation with 4MPBE and HPDP-B. The assignments of the numbered bands are reported in Table 1. c) SERS spectra of the nanosensor after 15 min exposure to 100 μM and 1 mM H_2O_2 as compared to the SERS spectra obtained from AuNP conjugated with 4MPh.

H_2O_2 in identical manner and it has been already utilized as a sensing molecule for intracellular H_2O_2 (Cheng et al., 2020). Nonetheless, the unprotected diols in 4MPBA are also prone to form boronate esters upon exposure to saccharides (Bull et al., 2013), which is the reason making 4MPBE a preferable choice for cell analysis. The results reported in Figure A1 of Appendix A confirm the influence of fructose and glucose on the SERS spectra of AuNP conjugated with 4MPBA. Upon incubation for 30 min in PBS solutions containing the monosaccharides at concentration of 5 mM, we noticed the increase of the band intensities at 998 and 1022 cm^{-1}, which is due to fructose and glucose binding to the boronic acid group and subsequent reorientation and charge distribution of the benzene ring (Sun et al. 2014, 2015). Conversely, 4MPBE is not affected by fructose.

3.2. Nanosensor calibration

Every sensor conceived for estimation of analytes requires a careful calibration before use. In cell biology and especially in reactions involving ROS, the meticulous consideration of the peculiar environment in which the sensor will operate is essential for the correctness of the calibration routine. Fig. 3a summarizes the steps of the experimental routine conceived for the calibration of our nanosensor. Firstly, the procedure cannot be limited to the mere exposure to aqueous solution at different concentrations of H_2O_2, but it necessitates the concurrent presence of the other species composing the physiological environment under investigation, which can react with part of the H_2O_2 in solution before it reaches the 4MPBE probe. In addition, the pH of the solution affects the concentration of hydrogen peroxide anions (HO_2^-) that react with 4MPBE and it may also affect the cross-section of some SERS bands (Scott and Carron 2016). Another key parameter to take into consideration is the time of exposure. As can be inferred by the name, ROS are highly reactive molecules, which generates irreversible modifications of the SAM. In the first step of cell sample preparation, the nanosensor is incubated in the cell culture for 30 min, during which the SAM is exposed and modified by endogenous H_2O_2. The results reported in Fig. 3b confirm that the H_2O_2-sensitive intensity ratio of the 1074 cm^{-1}

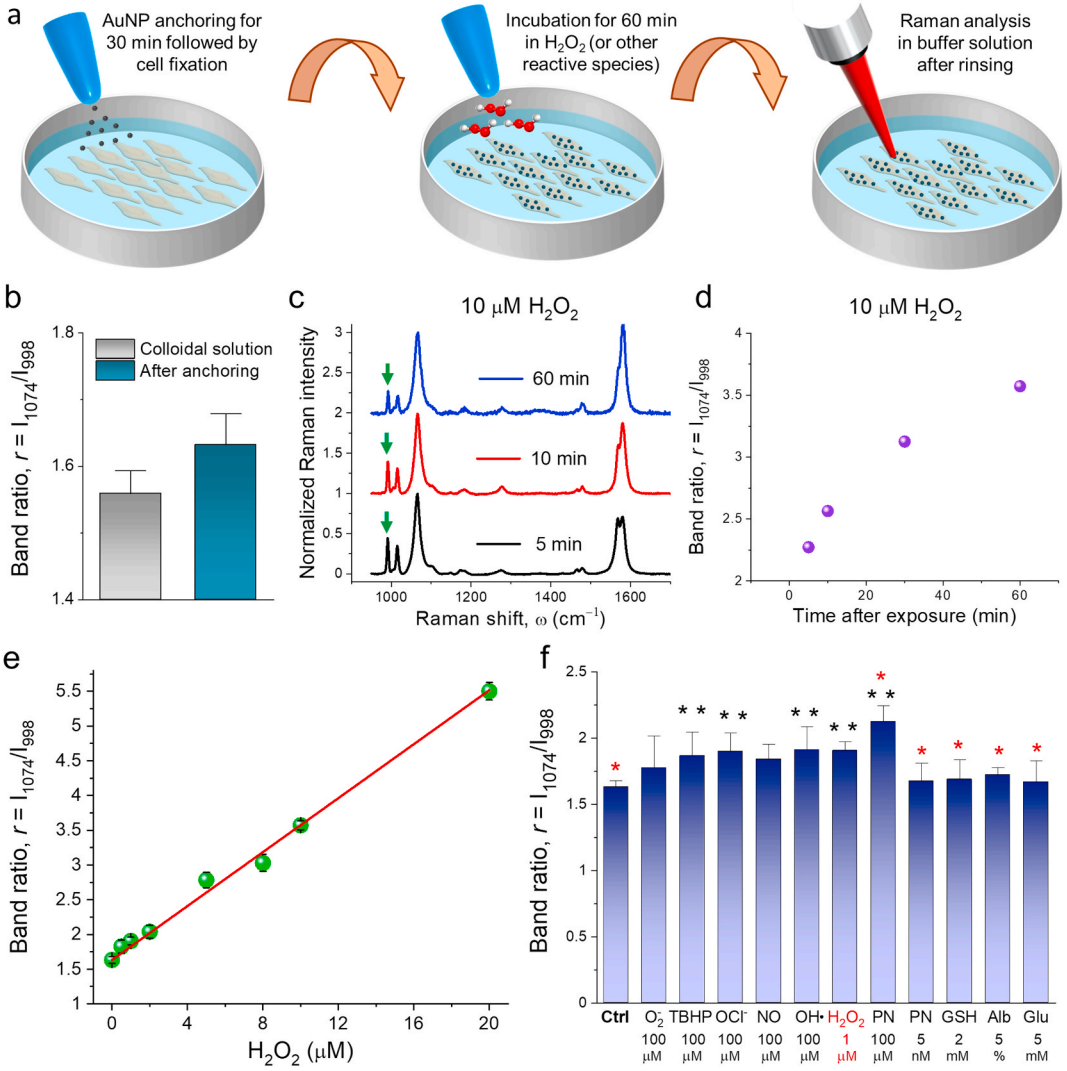

Fig. 3. Calibration procedure of the nanosensor. a) Steps of the calibration method of the nanosensor. b) Comparison of band ratios r before and after 30 min incubation for nanosensor anchoring on the cell surface. c) SERS spectra of the nanosensor exposed to buffer solution at constant concentration of H_2O_2 (10 μM) as collected at different incubation times. The green arrows indicate the band at 998 cm^{-1}, whose intensity is decreasing over time. d) Plot of the band ratio r as a function of exposure time to 10 μM H_2O_2. e) Calibration line of the band ratio r as a function of H_2O_2 concentration. The experimental SERS data were acquired after incubation of 60 min. f) SERS response of the nanosensor to different physiologically relevant reactive species (abbreviations defined in the paragraph Solutions containing biologically relevant species). Red asterisks indicate statistically meaningful difference from 1 μM H_2O_2, while double black asterisks show statistically meaningful difference from control (Ctrl) (ANOVA with Tukey's post hoc test, $p < 0.05$). (For interpretation of the references to colour in this figure legend, the reader is referred to the Web version of this article.)

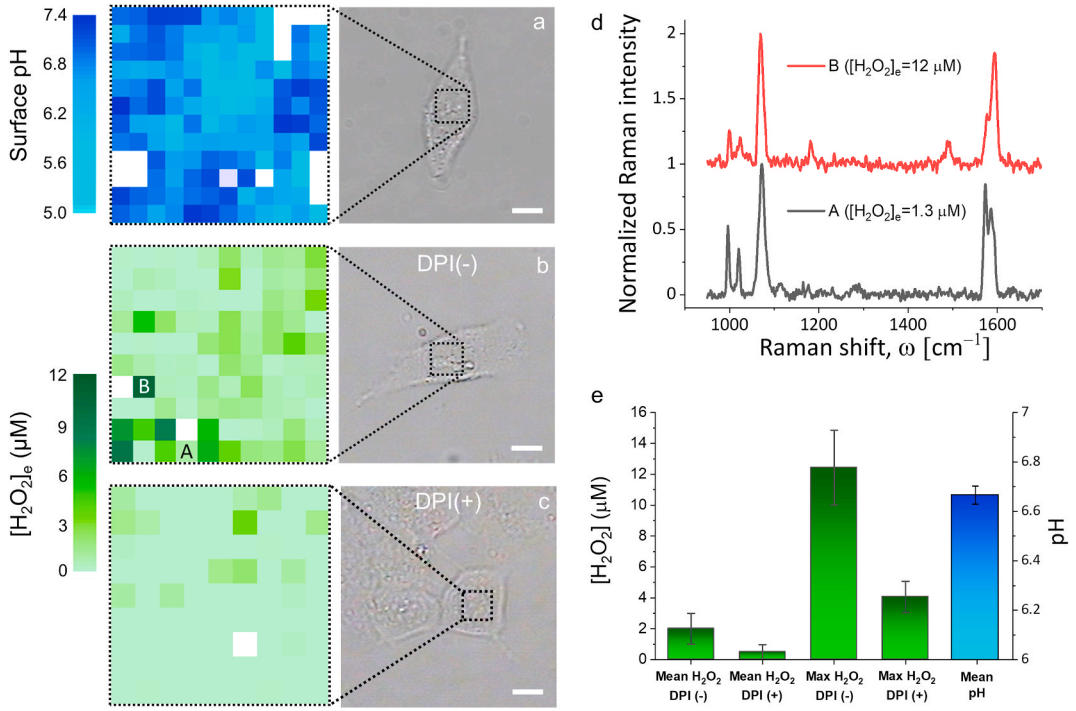

Fig. 4. SERS experiments on A549 cell samples. a) Hyperspectral map of surface pH collected from the location of the A549 cell shown in the bright-field image. b) Example of hyperspectral map of $[H_2O_2]_e$ collected from the surface of the A549 cell shown in the bright-field image. The extended leading side of this motile cell is on the left. The SERS spectra collected from the positions A and B are shown in (d). Scale bars in the bright-field images: 10 μm. Each square of the hyperspectral maps of pH or $[H_2O_2]_e$ corresponds to an actual spot of 700 nm diameter. c) Typical hyperspectral map of $[H_2O_2]_e$ collected from the surface of an A549 cell 60 min after addition of DPI. In (e) are reported the mean surface $[H_2O_2]_e$ and the typical maximum of $[H_2O_2]_e$ for each of the 2 investigated cases. In addition, also the mean surface pH is shown.

band to the 998 cm^{-1} band increases after anchoring of the nanosensor to the cells. Additionally, lipid peroxidation on plasma membrane occurs in real physiological conditions (Repetto et al., 2012) and it may affect the yield of the reaction between 4MPBE and H_2O_2. For all these reasons, we carried out the calibration of the nanosensor after anchoring it to the cell surface. The average SERS spectrum collected after anchoring is set as the zero reference to compare results of the calibration with those collected from experiments on living cells. As described in Fig. 3a, at the end of the incubation time with AuNP and rinsing, we fixed the cells to block the endogenous production of H_2O_2 and we added buffer solution at pre-determined constant concentration of H_2O_2. The results reported in Figure A1b of Appendix A confirm that the PBS buffer solution containing 2.5%GA-2%PA does not modify the 4MPBE SAM. During calibration, the pH was adjusted to 6.7 to mimic the typical A549 cell surface pH, previously quantified according to the protocol described in (Puppulin et al., 2018) (see also the results reported in the next section and in Fig. 4). After 60 min, we rinsed the sample with buffer solution and we collected SERS spectra from the modified SAM. This experimental routine was repeated on different cell samples incubated in solutions at different concentrations of H_2O_2. In Fig. 3c and d are reported the SERS data collected at different incubation times from the nanosensor exposed to 10 μM H_2O_2. Although the influence of H_2O_2 can be clearly detected after 5 min, in the present study, we selected 60 min as incubation time systematically used in our experiments, in order to maximize the modification of the SERS spectrum even at concentrations lower than 1 μM. In Fig. 3e, the results of the calibration are presented as SERS intensity ratio of the band at 1074 cm^{-1} to the band at 998 cm^{-1} (hereafter referred as *r*) as a function of H_2O_2 concentration. The regression analysis indicates linear dependence between the variables ($R^2 \geqslant 0.99$) and gave us the following equation:

$$[H_2O_2] = 5.18\, r - 8.45 \quad (1)$$

We used Eq. (1) to estimate $[H_2O_2]_e$ in μM on living cells. According to the results of the linear regression, the limit of detection (LOD) is estimated as 0.49 μM. In addition, we tested the selectivity of the nanosensor to H_2O_2 over a variety of biologically relevant species, including ROS like $O_2^{\cdot-}$, TBHP, OCl^-, ·NO, OH· and reactive molecules like PN, albumin, glucose and GSH. In a similar manner to the calibration routine, the SERS experiments on selectivity were performed after nanosensor anchoring to the cells, followed by cell fixation and exposure to the relevant reactive species. The comparison of the band ratios *r* calculated from each case is reported in Fig. 3f. The exposure to 1 μM H_2O_2 produced modification of the 4MPBE SAM equivalent to those induced by the other ROS at concentrations 100-fold higher (i.e., not expected on the cell surface). Conversely, the *r* ratios of albumin, glucose and GSH did not differ from the control. Separate discussion deserves the case of PN, which showed higher reactivity at concentration of 100 μM. A previous study on conjugated AuNP for detection of intracellular H_2O_2 showed that PN did not affect SAM made of phenylboronicacid (Qu et al., 2016). On the other hand, Sikora et al. showed that boronates as 4MPBE can be used to detect PN, since the rate constant ($k = 1.2 \times 10^6$ $M^{-1}s^{-1}$) measured for the reaction is high (Sikora et al., 2009). Peroxynitrites can be formed on the cell surface by the diffusion controlled reaction of ·NO with $O_2^{\cdot-}$, at rate constant within 4–16 × 10^9 $M^{-1}s^{-1}$, which is faster than the reaction of $O_2^{\cdot-}$ with extracellular superoxide dismutase (EC-SOD), producing H_2O_2 (i.e., rate constant within 1–2 × 10^9 $M^{-1}s^{-1}$). The main endogenous source of ·NO is the intracellular reaction of L-arginine with NADPH and oxygen, which is enzymatically catalyzed by several isoforms of nitric oxide synthase (Carballal et al., 2014). Although ·NO quickly reacts with $O_2^{\cdot-}$ produced in mitochondria and cytosol, it can also diffuse and permeate the plasma membrane to outcompete EC-SOD in reaction with $O_2^{\cdot-}$, leading to formation of PN on the cell surface. Nonetheless, physiological ·NO concentrations are expected to range from several pM up to about 5 nM (Hall and Garthwaite 2009; Szabó et al., 2007). Accordingly, the steady-state concentration of PN on the cell surface can be estimated in the low nanomolar range, at

most. Moreover, PN is a short-lived oxidant species that can readily react with many different species concentrated on the cell surface, such as lipids and thiol-containing proteins. As shown in Fig. 3f, exposure to 5 nM PN solutions did not modify the 4MPBE SAM of the nanosensor placed on the cell surface. Overall, these arguments and experimental evidence prove that the use of 4MPBE and the peculiar location of the nanosensor on the cell surface provide selectivity to H_2O_2.

3.3. SERS analysis of cell surface pH and H_2O_2

Preliminary experiments were conducted using the pH-sensitive nanosensor reported in (Puppulin et al., 2018), in order to quantify the pH to utilize for the calibration of the H_2O_2-sensitive nanosensor, as discussed in the previous section. Fig. 4a reports a representative hyperspectral map of surface pH collected from a A549 cell. The increase of proton concentration detected at nanometer distance from the outer plasma membrane is correlated to the activity of V-type ATP-dependent proton pumps (H^+-ATPase), sodium hydrogen exchangers (NHE), monocarboxylate transporters (MCTs) and carbonic anhydrases (CAs), which are particularly upregulated in most cancer histotypes (Cardone et al., 2005; Stock and Schwab 2009). These outcomes also confirmed that the laser power selected for SERS experiments did not damage the cell. In fact, the pH-sensitive 4MPBA can readily detect transient variation of proton concentration. In case of cell death during acquisition, the surface pH would have had to change dramatically, settling at the level of the buffer solution (i.e., 7.4). The spectroscopic analysis for quantifying H_2O_2 on A549 cells was rigorously carried out 60 min after the completion of the protocol for the nanosensor anchoring to the cells, which is the same incubation time used for the nanosensor calibration. This protocol of analysis is pivotal for the reproducibility of the measurements collected from different cell samples and for comparison between results of calibration and experiments on living cells. Considering that the cells are functioning at constant physiological regime (i.e., constant medium composition and temperature), production, diffusion and reaction of endogenous H_2O_2 occur continuously and simultaneously on the cell surface during incubation. Accordingly, H_2O_2 concentration gradients are established in the proximity of the cell surface, where the nanosensor is placed. Although the gradients of H_2O_2 can transiently fluctuate over time, the values estimated using this method represent the average concentrations of endogenous H_2O_2 over the incubation time at each analyzed location on the cell surface. For each measurement on living cells, the modifications of the 4MPBE SAM are equivalent to those observed after exposure to H_2O_2 standards at constant concentration for 60 min. Fig. 4b and c shows two typical hyperspectral maps of $[H_2O_2]_e$ collected from A549 cells incubated for 1 h in medium without and with addition of DPI (10 μM), respectively. The DPI is a potent inhibitor of the plasma membrane-associated NADPH oxidase complexes (NOXes), which are a family of oxygen- and NADPH-dependent oxidoreductases producing H_2O_2 on the cell surface (O'Donnell et al., 1993). The in-plane spatial resolution of each point of the hyperspectral maps can be approximated to the size of the laser spot, which is diffraction limited and is quantified to 700 nm (Puppulin et al., 2018). Conversely, the axial resolution is estimated as the maximum distance from the cell surface at which H_2O_2 is detected, which corresponds to the size of the nanosensor (i.e., about 90 nm). The SERS spectra in Fig. 4d confirm the modifications of the nanosensors anchored to the locations A and B of the cell in Fig. 4b, which were induced by $[H_2O_2]_e$ of 1.3 and 12 μM, respectively. As shown in Fig. 4e, according to the SERS results of $n = 3$ A549 cells from 3 different cell cultures without addition of DPI, the mean $[H_2O_2]_e$, the typical peak of $[H_2O_2]_e$ and the mean surface pH are estimated at 1.8 ± 0.5 μM, 12.4 ± 2.4 μM and 6.67 ± 0.03, respectively. In cells treated with DPI, the mean $[H_2O_2]_e$ and the mean peak of $[H_2O_2]_e$ are estimated at 0.74 ± 0.5 μM and 4.5 ± 1.6 μM, respectively. In the case of cells without inhibitor, the 38.4% of the measurements shows $[H_2O_2]_e$ lower than the nanosensor LOD, while in the case of DPI addition, this percentage rises to 63.6%. Moreover, without addition of DPI, 46.1% of the calculated values is higher than 1 μM, while $[H_2O_2]_e$ is higher than 6 μM only in few isolated spots (i.e., 17.8%), which are localized toward the extended leading side of this motile cell (i.e., the darkest spots on the map of Fig. 4b). With the addition of DPI, the percentages of the previous two cases drop to 25.6% and 0.4%, respectively. The abundant presence of surface H_2O_2 in cancer cells is predominantly achieved through upregulation of NOXes (Brandes et al., 2014; Groeger et al., 2009; Panday et al., 2015; Ushio-Fukai and Nakamura 2008). NOX homologues generate superoxide (O_2^-) and H_2O_2 in the extracellular compartments of different types of cells and tissues. Superoxide is readily enzymatically converted to H_2O_2 on the outer membrane by EC-SOD (isoform SOD3) (Fattman et al., 2003; Zelko et al., 2002). The generated H_2O_2 can enter the plasma membrane through water channel Aquaporin-3 (AQP3) (Miller et al., 2010) and activate specific redox signaling pathways for cell migration and growth. The NOX enzymes are spatially assembled in a highly regulated manner, typically in cholesterol- and sphingolipid-rich plasma membrane microdomains, such as lipid rafts and caveolae (Ushio-Fukai 2006; Woo et al., 2010). Overall, the comparison of the SERS data demonstrates that the effect of DPI is detected by the nanosensor. We hypothesize that the localized upregulations of H_2O_2 visualized in the hyperspectral maps may be correlated to NOXs activity. In recent years, electrochemical sensing of H_2O_2 produced by cells has been proposed using different modified electrodes, such as horseradish peroxidase supported on porous graphene or nitrogen/sulfur codoped graphene quantum dot/graphene hybrid nanosheets (Liu et al., 2017; Zhang et al., 2017). These biosensors can detect meaningful variation of H_2O_2 released by cells after stimulation (e.g., by ascorbic acid or unmodified Cadmium Telluride Quantum Dots). Although our method based on spectrophotometry does not exhibit similar sub-micromolar sensitivity and fast response, it is capable of probing a single cell and it has the advantage of locating the nanosensor in contact with the outer cell surface and detecting the H_2O_2 in the surrounding nano-environment (i.e., concentrations not diluted in μL of buffer). This peculiarity enabled to unveil high levels of H_2O_2 localized in sparse locations of the probed cell surface, which cannot be discriminated by the other methods developed so far.

3.4. Estimation of intracellular H_2O_2

In eukaryotic cells, intracellular levels of H_2O_2 are tightly regulated by several types of antioxidants, such as catalase, glutathione peroxidase, and the family of thioredoxin peroxidases, also known as peroxiredoxins. Beside the protective function against excessive oxidative stress in the cytoplasm, antioxidants are also assigned to create the proper conditions for signaling cell division, apoptosis, differentiation, or migration. Recent studies has brought to light the major role of peroxiredoxins in reducing up to the 90% of the cytoplasmic peroxides (Perkins et al., 2015). These enzymes possess highly conserved cysteine residues, which selectively and rapidly reduce H_2O_2 in a catalytic reaction scheme involving also thioredoxin (Choi et al., 2005). In HeLa cell lines, refined kinetic measurements revealed that peroxiredoxins with two conserved cysteine residues (2-cys-Prx) react with peroxides at rates 100 times faster than the rates of the other antioxidants (Choi et al., 2005; Huang and Sikes 2014; Veal et al., 2007). In addition, 2-Cys Prx are highly localized to the intracellular sites of H_2O_2 accumulation close to the plasma membrane, which indicates their involvement in switching off H_2O_2-signaling events. In the present study, we combine the experimental outcomes of our SERS analysis with those obtained through the application of advanced methods of redox biology. In particular, we extended to our nanosensor the analytical approach to estimate H_2O_2 concentration gradients across bio-membranes proposed by Antunes and Cadenas (2000) and adapted by Huang and Sikes (2014). As illustrated in the schematic of Fig. 5a, the activity of basal H_2O_2 in the proximity of the plasma membrane can be estimated using a kinetic model including the absorption of endogenously produced

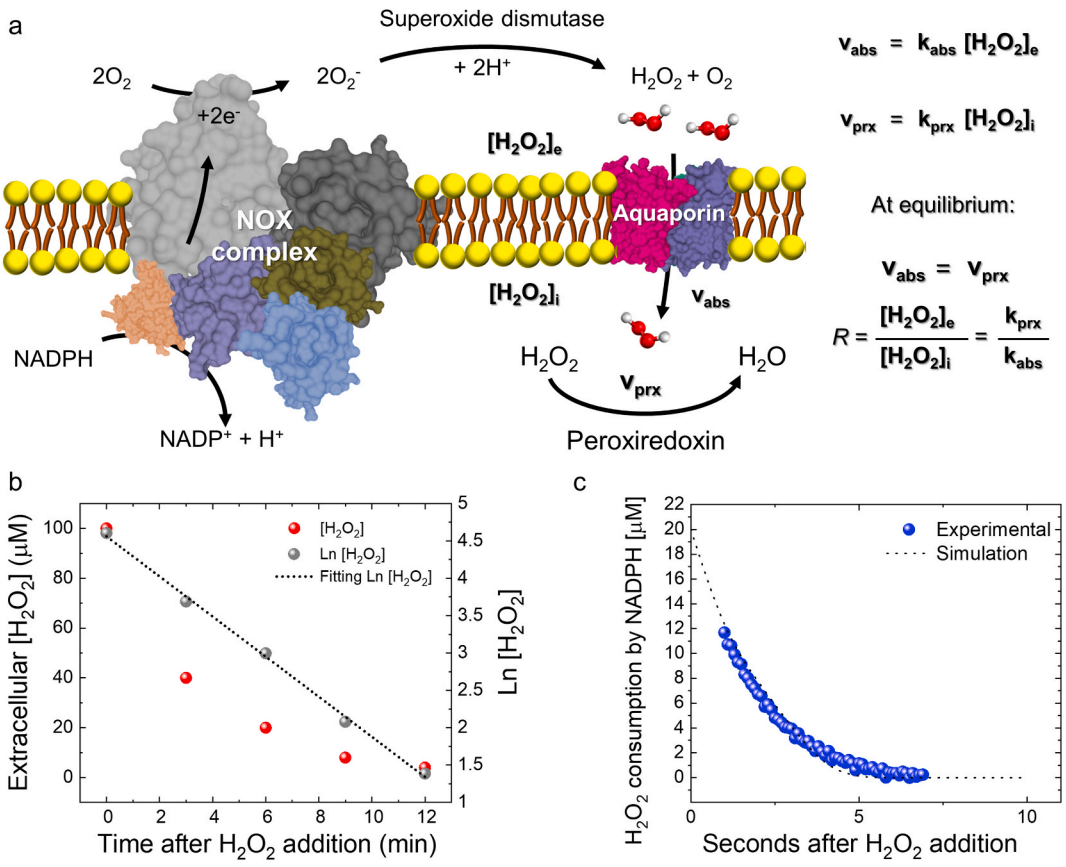

Fig. 5. Redox biology experiments for estimation of H_2O_2 gradients across the cell membrane. a) Explanatory schematic of the extracellular production of H_2O_2 by NOX complex, the absorption through Aquaporin channels and the reaction with intracellular peroxiredoxin. At steady-state condition, the ratio R between extracellular and intracellular concentrations of H_2O_2 can be estimated by the ratio between the rate constants k_{prx} and k_{abs}. b) Absorption of exogenous H_2O_2 added to intact A549 cells as measured by ABTS based assay. The slope of the natural logarithm of H_2O_2 variation as a function of time gives the kinetic rate constant k_{abs}. c) Typical results of experiments on A549 lysates incubated with 15 μM thioredoxin, 2 μM of TrxR, 300 μM NADPH and 20 μM H_2O_2. Reaction of H_2O_2 with peroxiredoxin of the lysate equals the depletion of NADPH measured by the absorption at 340 nm with a plate reader. We calculated k_{prx} with a numerical simulation of the experimental data based on the system of differential equations reported in (Huang and Sikes 2014) and Appendix A.

extracellular H_2O_2 and the reaction of scavenging by the predominant cytoplasmic antioxidant (i.e., peroxiredoxin in our case). At steady-state conditions, the rate of adsorption equals the rate of consumption by peroxiredoxin. When the cells are exposed to extracellular H_2O_2 in the micromolar range, the $[H_2O_2]_i$ is much lower than $[H_2O_2]_e$ and the most of the antioxidant pool is in the reduced form. Under these assumptions, both reactions of the model can be approximated to two pseudo-first order reactions (Huang and Sikes 2014; Low et al., 2007) and the gradient of H_2O_2 across the plasma membrane, $R = [H_2O_2]_e/[H_2O_2]_i$, can be expressed as the ratio between the two rate constants K_{prx} and K_{abs}. We determined the two kinetic rate constants by in-vitro experiments on A549 cell samples according to protocols reported in (Antunes and Cadenas 2000; Huang and Sikes 2014). Fig. 5b shows the trend of adorption of exogenous H_2O_2 added to intact A549 cells (i.e., initial concentration of 100 μM in buffer solution). The time-dependent concentration of extracellular H_2O_2 was measured monitoring the absorbance of 2,2-azino-bis(3-ethylbenzothiazoline-6-sulfonicacid) (ABTS). The slope of the natural logarithm of H_2O_2 versus time represents K_{abs} and it is estimated as equal to 4.5×10^{-12} s^{-1} $cell^{-1}$ L. In Fig. 5c is reported a typical outcome of experiments designed to estimate the reaction kinetics of H_2O_2 with the intracellular peroxiredoxins of A549 cells. Cell lysates treated with excess of thioredoxin, thioredoxin reductase and NADPH were analyzed after addition of a bolus of H_2O_2 producing an initial concentration of 20 μM. The consumption of H_2O_2 by peroxiredoxins is equivalent to the depletion of NADPH, which can be monitored by measuring the variation of absorbance at 340 nm. The pseudo first-order kinetic rate constant K_{prx} represents the average concentration of the peroxiredoxins pool in the A549 cell lysate multiplied by the typical second-order rate constant of the reaction between the antioxidant and H_2O_2. It was determined by fitting the experimental data using a computational routine adapted from the method introduced in (Huang and Sikes 2014) and reported in detail in Appendix A. We found a K_{prx} of $1.1 \pm 0.06 \times 10^{-8}$ s^{-1} $cell^{-1}$ L. Based on these results, we quantified $R = 2444$. The $[H_2O_2]_e$ obtained by SERS analysis divided by R estimates the respective $[H_2O_2]_i$ beyond the plasma membrane. According to our analysis of $n = 3$ A549 cells, the mean $[H_2O_2]_i$ is 0.7 ± 0.2 nM and the peak of $[H_2O_2]_i$ is 5.1 ± 1 nM. These levels of $[H_2O_2]_i$ are calculated using the average kinetic constant of peroxiredoxins in A549 cells. Nonetheless, PrxI and PrxII, which are the predominant members of 2-cys-Prx localized in the cytoplasm, can be transiently inactivated during signaling by phosphorylation of tyrosine-194 and hyperoxidation, respectively (Woo et al., 2010). The possible occurrence of highly localized inactivation of the antioxidant may induce transient accumulation of H_2O_2, exceeding the concentration estimated in the present study. For this reason, further investigation and improvement of the technique are required to unveil any transient peak of H_2O_2.

4. Conclusion

In summary, this study introduces a new nanosensor for SERS measurements of endogenous H_2O_2 on the outer surface of cells with high spatial resolution. The peculiarity of this method is the positioning of the

sensor at nanometer distance from the cell surface, namely in the very shallow region of the extracellular milieu in which physiologically meaningful gradients of H_2O_2 occur. Hyperspectral mapping of the cell surface by SERS enabled us to retrieve localized spots at higher concentration of H_2O_2, up to 12 μM, which we hypothesize to be associated to clustering and upregulation of NOX complexes. We also propose the calculation of physiological relevant concentrations of intracellular H_2O_2 using a combination of SERS analyses and redox biology experiments that estimate gradients of H_2O_2 across biological cell membranes. This novel approach may be useful for the study of actual H_2O_2 concentrations involved in cell proliferation or death, which are fundamental to fully elucidate physiological processes and to design new therapeutic strategies.

CRediT authorship contribution statement

Shigekuni Hosogi: Conceptualization, Investigation, Data curation. **Yoshinori Marunaka:** Resources, Writing - review & editing. **Eishi Ashihara:** Resources, Writing - review & editing. **Tadaaki Yamada:** Resources, Investigation. **Ayumi Sumino:** Resources, Investigation. **Hideo Tanaka:** Resources, Writing - review & editing. **Leonardo Puppulin:** Conceptualization, Methodology, Software, Data curation, Visualization, Validation, Supervision, Writing - original draft.

Declaration of competing interest

The authors declare that they have no known competing financial interests or personal relationships that could have appeared to influence the work reported in this paper.

Acknowledgments

This work was supported by World Premier International Research Center Initiative (WPI), MEXT, Japan and the Grant-in-Aid for Scientific Research (C) Number 19K05228 of The Japanese Society for the Promotion of Science (L.P.).

Appendix A. Supplementary data

Supplementary data to this article can be found online at https://doi.org/10.1016/j.bios.2021.113077.

References

Antunes, F., Cadenas, E., 2000. Estimation of H2O2 gradients across biomembranes. FEBS Lett. 475 (2), 121–126.
Bauer, G., 2012. Tumor cell-protective catalase as a novel target for rational therapeutic approaches based on specific intercellular ROS signaling. Anticancer Res. 32 (7), 2599–2624.
Behrend, L., Henderson, G., Zwacka, R., 2003. Reactive Oxygen Species in Oncogenic Transformation. Portland Press Ltd.
Belousov, V.V., Fradkov, A.F., Lukyanov, K.A., Staroverov, D.B., Shakhbazov, K.S., Terskikh, A.V., Lukyanov, S., 2006. Genetically encoded fluorescent indicator for intracellular hydrogen peroxide. Nat. Methods 3 (4), 281.
Brandes, R.P., Weissmann, N., Schröder, K., 2014. Nox family NADPH oxidases: molecular mechanisms of activation. Free Radic. Biol. Med. 76, 208–226.
Bull, S.D., Davidson, M.G., Van den Elsen, J.M., Fossey, J.S., Jenkins, A.T.A., Jiang, Y.-B., Kubo, Y., Marken, F., Sakurai, K., Zhao, J., 2013. Exploiting the reversible covalent bonding of boronic acids: recognition, sensing, and assembly. Acc. Chem. Res. 46 (2), 312–326.
Burdo, R.H., Rice-Evans, C., 1989. Free radicals and the regulation of mammalian cell proliferation. Free Radic. Res. Commun. 6 (6), 345–358.
Carballal, S., Bartesaghi, S., Radi, R., 2014. Kinetic and mechanistic considerations to assess the biological fate of peroxynitrite. Biochim. Biophys. Acta Gen. Subj. 1840 (2), 768–780.
Cardone, R.A., Casavola, V., Reshkin, S.J., 2005. The role of disturbed pH dynamics and the Na+/H+ exchanger in metastasis. Nat. Rev. Canc. 5 (10), 786–795.
Cash, T.P., Pan, Y., Simon, M.C., 2007. Reactive oxygen species and cellular oxygen sensing. Free Radic. Biol. Med. 43 (9), 1219–1225.
Centeno, S.P., Lopez-Tocon, I., Roman-Perez, J., Arenas, J.F., Soto, J., Otero, J.C., 2012. Franck–condon dominates the surface-enhanced Raman scattering of 3-methylpyridine: propensity rules of the charge-transfer mechanism under reduced symmetry. J. Phys. Chem. C 116 (44), 23639–23645.
Chen, G., Chen, Z., Hu, Y., Huang, P., 2011. Inhibition of mitochondrial respiration and rapid depletion of mitochondrial glutathione by β-phenethyl isothiocyanate: mechanisms for anti-leukemia activity. Antioxidants Redox Signal. 15 (12), 2911–2921.
Cheng, W., Tang, P., He, X., Xing, X., Xing, M., Lu, L., Ju, P., Wang, Y., Liu, S., Lu, X., 2020. Dynamic Monitoring and Quantitative Characterization of Intracellular H2O2 Content by Using SERS Based Boric Acid Nanoprobe. Talanta, 120863.
Choi, M.H., Lee, I.K., Kim, G.W., Kim, B.U., Han, Y.-H., Yu, D.-Y., Park, H.S., Kim, K.Y., Lee, J.S., Choi, C., 2005. Regulation of PDGF signalling and vascular remodelling by peroxiredoxin II. Nature 435 (7040), 347–353.
D'Autréaux, B., Toledano, M.B., 2007. ROS as signalling molecules: mechanisms that generate specificity in ROS homeostasis. Nat. Rev. Mol. Cell Biol. 8 (10), 813.
Fattman, C.L., Schaefer, L.M., Oury, T.D., 2003. Extracellular superoxide dismutase in biology and medicine. Free Radic. Biol. Med. 35 (3), 236–256.
Finkel, T., 2011. Signal transduction by reactive oxygen species. J. Cell Biol. 194 (1), 7–15.
Fruehauf, J.P., Meyskens, F.L., 2007. Reactive oxygen species: a breath of life or death? Clin. Canc. Res. 13 (3), 789–794.
Gorrini, C., Harris, I.S., Mak, T.W., 2013. Modulation of oxidative stress as an anticancer strategy. Nat. Rev. Drug Discov. 12 (12), 931–947.
Groeger, G., Quiney, C., Cotter, T.G., 2009. Hydrogen peroxide as a cell-survival signaling molecule. Antioxidants Redox Signal. 11 (11), 2655–2671.
Gupta, S.C., Hevia, D., Patchva, S., Park, B., Koh, W., Aggarwal, B.B., 2012. Upsides and downsides of reactive oxygen species for cancer: the roles of reactive oxygen species in tumorigenesis, prevention, and therapy. Antioxidants Redox Signal. 16 (11), 1295–1322.
Hall, C.N., Garthwaite, J., 2009. What is the real physiological NO concentration in vivo? Nitric Oxide 21 (2), 92–103.
Huang, B.K., Langford, T.F., Sikes, H.D., 2016. Using sensors and generators of H2O2 to elucidate the toxicity mechanism of piperlongumine and phenethyl isothiocyanate. Antioxidants Redox Signal. 24 (16), 924–938.
Huang, B.K., Sikes, H.D., 2014. Quantifying intracellular hydrogen peroxide perturbations in terms of concentration. Redox biology 2, 955–962.
Jencks, W.P., Carriuolo, J., 1960. Reactivity of nucleophilic reagents toward esters. J. Am. Chem. Soc. 82 (7), 1778–1786.
Ji, W., Xue, X., Ruan, W., Wang, C., Ji, N., Chen, L., Li, Z., Song, W., Zhao, B., Lombardi, J.R., 2011. Scanned chemical enhancement of surface-enhanced Raman scattering using a charge-transfer complex. Chem. Commun. 47 (8), 2426–2428.
Lee, H.M., Kim, M.S., Kim, K., 1994. Surface-enhanced Raman scattering of ortho-and para-mercaptophenols in silver sol. Vib. Spectrosc. 6 (2), 205–214.
Li, S., Zhou, Q., Chu, W., Zhao, W., Zheng, J., 2015. Surface-enhanced Raman scattering behaviour of 4-mercaptophenyl boronic acid on assembled silver nanoparticles. Phys. Chem. Chem. Phys. 17 (27), 17638–17645.
Lin, V.S., Dickinson, B.C., Chang, C.J., 2013. Boronate-based fluorescent probes: imaging hydrogen peroxide in living systems. Methods Enzymol. 19–43 (Elsevier).
Liou, G.-Y., Storz, P., 2010. Reactive oxygen species in cancer. Free Radic. Res. 44 (5), 479–496.
Lippert, A.R., Van de Bittner, G.C., Chang, C.J., 2011. Boronate oxidation as a bioorthogonal reaction approach for studying the chemistry of hydrogen peroxide in living systems. Acc. Chem. Res. 44 (9), 793–804.
Liu, Y., Liu, X., Guo, Z., Hu, Z., Xue, Z., Lu, X., 2017. Horseradish peroxidase supported on porous graphene as a novel sensing platform for detection of hydrogen peroxide in living cells sensitively. Biosens. Bioelectron. 87, 101–107.
Low, F.M., Hampton, M.B., Peskin, A.V., Winterbourn, C.C., 2007. Peroxiredoxin 2 functions as a noncatalytic scavenger of low-level hydrogen peroxide in the erythrocyte. Blood 109 (6), 2611–2617.
Lyublinskaya, O., Antunes, F., 2019. Measuring intracellular concentration of hydrogen peroxide with the use of genetically encoded H2O2 biosensor HyPer. Redox biology 24, 101200.
Lyublinskaya, O., Ivanova, J.S., Pugovkina, N., Kozhukharova, I., Kovaleva, Z., Shatrova, A., Aksenov, N., Zenin, V., Kaulin, Y.A., Gamaley, I., 2017. Redox environment in stem and differentiated cells: a quantitative approach. Redox biology 12, 758–769.
Miller, E.W., Albers, A.E., Pralle, A., Isacoff, E.Y., Chang, C.J., 2005. Boronate-based fluorescent probes for imaging cellular hydrogen peroxide. J. Am. Chem. Soc. 127 (47), 16652–16659.
Miller, E.W., Dickinson, B.C., Chang, C.J., 2010. Aquaporin-3 mediates hydrogen peroxide uptake to regulate downstream intracellular signaling. Proc. Natl. Acad. Sci. Unit. States Am. 107 (36), 15681–15686.
O'Donnell, V.B., Tew, D.G., Jones, O.T., England, P., 1993. Studies on the inhibitory mechanism of iodonium compounds with special reference to neutrophil NADPH oxidase. Biochem. J. 290 (1), 41–49.
Panday, A., Sahoo, M.K., Osorio, D., Batra, S., 2015. NADPH oxidases: an overview from structure to innate immunity-associated pathologies. Cell. Mol. Immunol. 12 (1), 5.
Paravicini, T.M., Touyz, R.M., 2008. NADPH oxidases, reactive oxygen species, and hypertension: clinical implications and therapeutic possibilities. Diabetes Care 31 (Suppl. 2), S170–S180.
Peng, R., Si, Y., Deng, T., Zheng, J., Li, J., Yang, R., Tan, W., 2016. A novel SERS nanoprobe for the ratiometric imaging of hydrogen peroxide in living cells. Chem. Commun. 52 (55), 8553–8556.
Perkins, A., Nelson, K.J., Parsonage, D., Poole, L.B., Karplus, P.A., 2015. Peroxiredoxins: guardians against oxidative stress and modulators of peroxide signaling. Trends Biochem. Sci. 40 (8), 435–445.

Puppulin, L., Hosogi, S., Sun, H., Matsuo, K., Inui, T., Kumamoto, Y., Suzaki, T., Tanaka, H., Marunaka, Y., 2018. Bioconjugation strategy for cell surface labelling with gold nanostructures designed for highly localized pH measurement. Nat. Commun. 9 (1), 5278.
Qu, L.-L., Liu, Y.-Y., He, S.-H., Chen, J.-Q., Liang, Y., Li, H.-T., 2016. Highly selective and sensitive surface enhanced Raman scattering nanosensors for detection of hydrogen peroxide in living cells. Biosens. Bioelectron. 77, 292–298.
Repetto, M., Semprine, J., Boveris, A., 2012. Lipid Peroxidation: Chemical Mechanism, Biological Implications and Analytical Determination. chapter.
Robinson, K.M., Beckman, J.S., 2005. Synthesis of peroxynitrite from nitrite and hydrogen peroxide. Methods Enzymol. 396, 207–214.
Scheit, K., Bauer, G., 2015. Direct and indirect inactivation of tumor cell protective catalase by salicylic acid and anthocyanidins reactivates intercellular ROS signaling and allows for synergistic effects. Carcinogenesis 36 (3), 400–411.
Schumacker, P.T., 2015. Reactive oxygen species in cancer: a dance with the devil. Canc. Cell 27 (2), 156–157.
Scott, B.L., Carron, K.T., 2016. Dynamic Raman scattering studies of coated gold nanoparticles: 4-mercaptopyridine, 4-mercaptophenol, and benzenethiol. J. Phys. Chem. C 120 (37), 20905–20913.
Sies, H., 2017. Hydrogen peroxide as a central redox signaling molecule in physiological oxidative stress: oxidative eustress. Redox biology 11, 613–619.
Sikora, A., Zielonka, J., Lopez, M., Joseph, J., Kalyanaraman, B., 2009. Direct oxidation of boronates by peroxynitrite: mechanism and implications in fluorescence imaging of peroxynitrite. Free Radic. Biol. Med. 47 (10), 1401–1407.
Simon, H.-U., Haj-Yehia, A., Levi-Schaffer, F., 2000. Role of reactive oxygen species (ROS) in apoptosis induction. Apoptosis 5 (5), 415–418.
Son, Y., Cheong, Y.-K., Kim, N.-H., Chung, H.-T., Kang, D.G., Pae, H.-O., 2011. Mitogen-activated protein kinases and reactive oxygen species: how can ROS activate MAPK pathways? J. Signal Transduct. 2011, 6. https://doi.org/10.1155/2011/792639. Article ID: 792639.
Stock, C., Schwab, A., 2009. Protons make tumor cells move like clockwork. Pflueg. Arch. Eur. J. Physiol. 458 (5), 981–992.
Stone, J.R., Yang, S., 2006. Hydrogen peroxide: a signaling messenger. Antioxidants Redox Signal. 8 (3–4), 243–270.
Sun, F., Bai, T., Zhang, L., Ella-Menye, J.-R., Liu, S., Nowinski, A.K., Jiang, S., Yu, Q., 2014. Sensitive and fast detection of fructose in complex media via symmetry breaking and signal amplification using surface-enhanced Raman spectroscopy. Anal. Chem. 86 (5), 2387–2394.
Sun, F., Ella-Menye, J.-R., Galvan, D.D., Bai, T., Hung, H.-C., Chou, Y.-N., Zhang, P., Jiang, S., Yu, Q., 2015. Stealth surface modification of surface-enhanced Raman scattering substrates for sensitive and accurate detection in protein solutions. ACS Nano 9 (3), 2668–2676.
Szabó, C., Ischiropoulos, H., Radi, R., 2007. Peroxynitrite: biochemistry, pathophysiology and development of therapeutics. Nat. Rev. Drug Discov. 6 (8), 662–680.
Taniyama, Y., Griendling, K.K., 2003. Reactive oxygen species in the vasculature: molecular and cellular mechanisms. Hypertension 42 (6), 1075–1081.
Touyz, R.M., 2005. Reactive oxygen species as mediators of calcium signaling by angiotensin II: implications in vascular physiology and pathophysiology. Antioxidants Redox Signal. 7 (9–10), 1302–1314.
Trachootham, D., Zhou, Y., Zhang, H., Demizu, Y., Chen, Z., Pelicano, H., Chiao, P.J., Achanta, G., Arlinghaus, R.B., Liu, J., 2006. Selective killing of oncogenically transformed cells through a ROS-mediated mechanism by β-phenylethyl isothiocyanate. Canc. Cell 10 (3), 241–252.
Ushio-Fukai, M., 2006. Localizing NADPH oxidase–derived ROS. Sci. STKE 2006 (349), re8 re8.
Ushio-Fukai, M., Nakamura, Y., 2008. Reactive oxygen species and angiogenesis: NADPH oxidase as target for cancer therapy. Canc. Lett. 266 (1), 37–52.
Veal, E.A., Day, A.M., Morgan, B.A., 2007. Hydrogen peroxide sensing and signaling. Mol. Cell 26 (1), 1–14.
Waris, G., Ahsan, H., 2006. Reactive oxygen species: role in the development of cancer and various chronic conditions. J. Carcinog. 5, 14.
Woo, H.A., Yim, S.H., Shin, D.H., Kang, D., Yu, D.-Y., Rhee, S.G., 2010. Inactivation of peroxiredoxin I by phosphorylation allows localized H2O2 accumulation for cell signaling. Cell 140 (4), 517–528.
Zelko, I.N., Mariani, T.J., Folz, R.J., 2002. Superoxide dismutase multigene family: a comparison of the CuZn-SOD (SOD1), Mn-SOD (SOD2), and EC-SOD (SOD3) gene structures, evolution, and expression. Free Radic. Biol. Med. 33 (3), 337–349.
Zhang, T., Gu, Y., Li, C., Yan, X., Lu, N., Liu, H., Zhang, Z., Zhang, H., 2017. Fabrication of novel electrochemical biosensor based on graphene nanohybrid to detect H2O2 released from living cells with ultrahigh performance. ACS Appl. Mater. Interfaces 9 (43), 37991–37999.